

Frequency Increase and Damping of Nonlinear Electron Plasma Oscillations in Cylindrical Symmetry

J. R. Marquès,¹ F. Dorchies,¹ P. Audebert,¹ J. P. Geindre,¹ F. Amiranoff,¹ J. C. Gauthier,¹ G. Hammoniaux,²

A. Antonetti,² P. Chessa,³ P. Mora,³ and T. M. Antonsen, Jr.⁴

¹LULI, Ecole Polytechnique–CNRS, 91128 Palaiseau, France

²LOA, ENSTA, Ecole Polytechnique–CNRS, 91128 Palaiseau, France

³CPTH, Ecole Polytechnique–CNRS, 91128 Palaiseau, France

⁴IRPDEEP, University of Maryland, College Park, Maryland 20742

(Received 29 October 1996)

Radial electron plasma oscillations excited by a laser wake field are measured by frequency domain interferometry. In the nonlinear regime we observe two important effects: (i) an increase of the oscillation frequency and (ii) the damping of the oscillation in a few plasma periods. Simulations show that this last effect is related to the presence of a steep radial density gradient near the focus edge. [S0031-9007(97)03054-8]

PACS numbers: 52.40.Nk, 52.35.Mw, 52.75.Di

The electrostatic field associated with an electron plasma wave (EPW) can reach hundreds of GV/m and can have a relativistic phase velocity, making it very attractive in compact high energy particle accelerators or sources [1]. The ponderomotive force of an intense laser pulse can excite such waves via the laser beat-wave (LBW) [2], the laser wake field (LWF) [2] or the self-resonant LWF (SRLWF) processes [3]. Several experiments have observed the acceleration of injected electrons by the LBW [4–7] and the LWF [8], or of background electrons by the SRLWF [8,9]. Electric fields of the order of the GV/m for the LBW or the LWF, and of 100 GV/m for the SRLWF have been produced. An overview of these methods and experiments can be found in Ref. [10]. If these experiments have demonstrated the feasibility of each concept, direct measurements of the EPW have been done only in LBW experiments [5,7].

Radial (cylindrical) electron density oscillations produced by the LWF process have recently been observed by frequency domain interferometry of short laser pulses. The oscillations have been measured with a temporal resolution much better than the electron plasma period [11,12] and spatial resolution along the radius [11]. In this Letter we present measurements of the nonlinear frequency shift predicted by Dawson [13] and of the damping of the radial oscillations. The results are compared with numerical simulations.

The basic theory of the cylindrical LWF, the frequency domain interferometry diagnostic, the experimental setup and procedure have been presented in detail in a previous publication [11]. We summarize here the experimental parameters. The LOA 10 Hz Ti:sapphire laser delivers pulses with an energy of 40 mJ, a duration of 130 ± 10 fs (FWHM), and a wavelength of $0.8 \mu\text{m}$. 20% of this incoming beam is used to create the probe beam. It is frequency doubled and sent to a Michelson interferometer to generate two collinear pulses of adjustable time

separation. The time delay between the pump and the probe pulses is varied with a delay line. The pump and probe pulses are collinearly propagated and focused in a chamber backfilled with helium gas. The gas pressure is controlled with a precision of ± 0.001 mbar by a capacitance manometer. The pump beam has a $\sigma = 6 \pm 1 \mu\text{m}$ focal spot radius ($1/e$ in intensity), while the probe radius is $140 \mu\text{m}$. The maximum pump intensity is $2 \times 10^{17} \text{ W/cm}^2$, leading to fully ionized helium gas around the focus [14]. The focal plane is imaged on the slit of a spectrometer. The time separation of the two probe pulses is adjusted to $1.5T_{\text{pe}}$ ($T_{\text{pe}} = 2\pi/\omega_{\text{pe}}$ is the EPW period for fully ionized helium), so that the phase difference between the two pulses is due to the peak to peak density perturbation. The spectrometer grating stretches the two probe pulses (≈ 60 ps) and makes them overlap in time. The temporal beating creates a system of fringes in the frequency domain. The position of the fringes depends on the relative phase between the two pulses. The fringes at the output of the spectrometer are recorded on a 16 bit charge-coupled device camera. The horizontal axis gives the position of the fringes (related to the density perturbation), and the vertical axis gives a one-dimensional spatial (radial) resolution.

A typical result of the relative phase measurement is shown in Fig. 1. The horizontal axis is the time delay between the pump and the probe pulses, while the vertical axis is the spectrometer slit axis. The left part 1(A) of this image corresponds to the case where the pump pulse is between the two probe pulses. The measured phase shift comes from the plasma formation. Its amplitude and spatial extent represent the integration along the laser axis of the regions one and two times ionized. The right part 1(B) of the image starts when the second probe pulse enters the plasma. The continuous phase shift vanishes, and only the oscillating phase shift coming from the plasma perturbation (due to the EPW) remains. Because

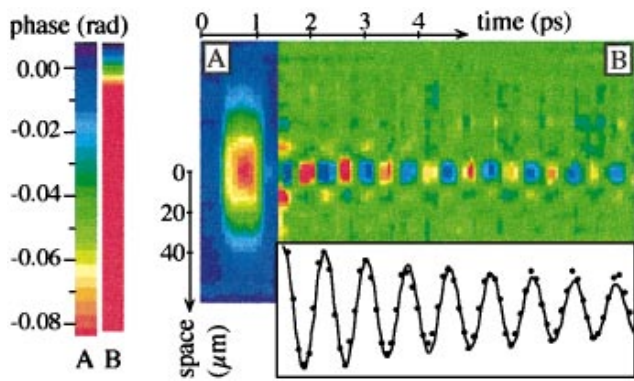


FIG. 1(color). Typical result of the phase shift measurement. Parts (A) and (B) have different color scales. The bottom graph is a line out of part (B) along the laser axis. $n_e = 2.47 \times 10^{16} \text{ cm}^{-3}$.

the laser wake field is significant only in regions of high laser intensity, the phase shift in part 1(B) has a much smaller extent (pump focal spot diameter) than in part 1(A). More details on these spatial profiles can be found in Ref. [11].

Figure 2 gives the maximum phase shift measured on the laser axis, as a function of the electron density (assuming a fully ionized He gas). Each point is an average of 40 shots at 10 Hz. It shows the LWF quaresonance in δn . The relation between the phase and the density perturbation is obtained by integrating the perturbation along the laser axis. For a cylindrical EPW [11], δn is proportional to $\sigma^{-4} = \sigma_0^{-4} (1 + z^2/z_R^2)^{-2}$, so that the phase difference is $\Delta\phi = \pi^2 (\delta n_{\text{max}}/n_{c1}) (z_R/\lambda_1) \exp[-(\omega_{pe} \tau/2)^2]$, where λ_1 and n_{c1} are the probe wavelength and its critical density, and where $z_R = 2\pi\sigma^2/\lambda$ is the pump Rayleigh length. The solid line is a numerical fit using the expression of $\delta n_r = A\omega_{pe} \tau \exp[-2(\omega_{pe} \tau/2)^2]$ obtained from the linear theory [15], where the adjustable parameters are an amplitude A and the pump and the probe pulse duration τ . The factor 2 in the exponential comes from the

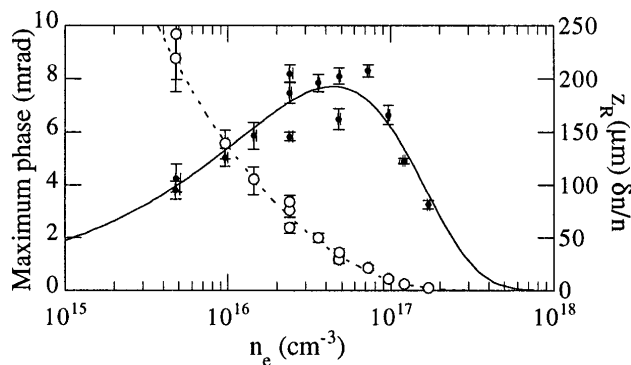


FIG. 2. Maximum phase shift (filled circles) on the laser axis versus the electron density and numerical fit (solid line) of the form $A\omega_{pe} \tau \exp[-2(\omega_{pe} \tau/2)^2]$; relative density perturbation times the pump Rayleigh length (empty circles) and numerical fit (dashed line) of the form $B \exp[-C\omega_{pe}^2]/\omega_{pe}$.

temporal convolution induced by the probe pulse temporal envelope: For a Gaussian envelope and a sinusoidal perturbation, the convolution decreases the phase shift by $\exp[(\omega_{pe} \tau_1/2)^2]$, where τ_1 is the half width at $1/e$ in intensity of the probe pulse. The best fit is obtained for $\tau = 84 \text{ fs}$ (FWHM = 140 fs), in good agreement with the laser pulse duration. The product $z_R \delta n/n_e$ obtained from the above formula is presented in Fig. 2 (empty circles). The dashed line is a numerical fit using the expression of $\delta n/n_e = B \exp[-C\omega_{pe}^2]/\omega_{pe}$ obtained from the linear theory [11,15]. In opposition with longitudinal oscillations where both δn and $\delta n/n_e$ present a resonance, one can see that radial oscillations have no resonance in $\delta n/n_e$, and that the lower is n_e , the larger is $\delta n/n_e$. In this experiment $z_R \approx 100 \mu\text{m}$ so that the relative density perturbation at the focus is $\delta n/n_e \approx 10\%$ at the resonance in δn ($n_e \approx 10^{17} \text{ cm}^{-3}$) and reaches $\delta n/n_e \approx 100\%$ for $n_e \leq 10^{16} \text{ cm}^{-3}$.

An example of the phase shift (along the laser axis) versus time (pump-probe delay) is presented on the line-out of Fig. 1. We applied to these curves a numerical fit of the form $\Delta\phi_{\text{max}} \exp[-\gamma(t - t_0)] \sin[\omega_p(t - t_0)]$. The damping rate γ and the frequency ω_p of the electron oscillations are deduced from these fits. The relative difference $(\omega_p - \omega_{pe})/\omega_{pe}$ between the measured frequency ω_p and the theoretical linear plasma frequency is presented in Fig. 3 as a function of the electron density n_e . A positive shift (frequency higher than the theoretical linear frequency) can be clearly seen. It increases when the electron density decreases, and reaches 5% for $n_e \approx 10^{16} \text{ cm}^{-3}$. The results of the numerical code WAKE originally developed by Mora and Antonsen [16] have been added on this figure (empty triangles). It is a 2D (cylindrical), fully relativistic particle-in-cell code, where the laser field acts on the particles via the ponderomotive force. The new version of the code used here simulates also the plasma formation (by tunneling ionization), the propagation of the two frequency doubled probe pulses, the imaging lens, and the time domain

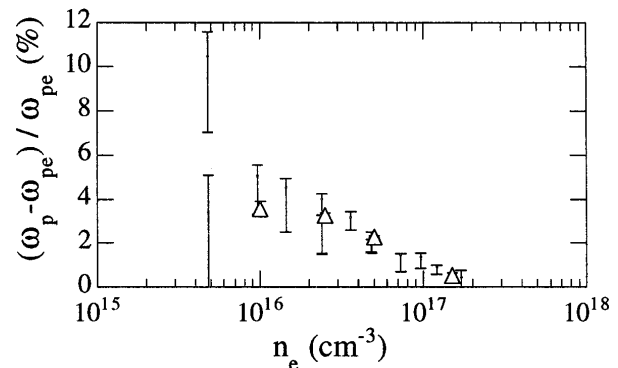


FIG. 3. Shift of the electron plasma frequency as a function of the electron density. The empty triangles are the results of the code WAKE.

interferometry. Only the residual energy produced during the ionization is not self-defined but controlled by giving to the generated electrons a Maxwellian radial velocity distribution. The frequency shift calculated by the code is in good agreement with the measurements. Let us note that even if the density perturbation is nonlinear, the code indicates that the measured phase shift still has a sinusoidal time evolution and a radial profile very close to the one obtained from linear theory. This is due to the temporal convolution over the probe pulses, and to the integration along the laser axis. Applying the above fit on much later periods (where the EPW amplitude is smaller) shows that the shift disappears, both in the experiment and in the simulations. This indicates that the shift does not come from an uncertainty in the pressure measurement or from the delay-line calibration, but is related to the nonlinear amplitude of the EPW. Few mechanisms can modify the electron plasma frequency. In a hot plasma the frequency increases: $\omega_p^2 = \omega_{pe}^2 + 3k^2 v_{th}^2$. Assuming $k \approx 2/\sigma$ leads to $\Delta\omega_p/\omega_{pe} \approx 6v_{th}^2/(\sigma^2\omega_{pe}^2)$. With $n_e = 10^{16} \text{ cm}^{-3}$, $T_e = 50 \text{ eV}$, and $\sigma = 6 \mu\text{m}$ the shift should be $\Delta\omega_p/\omega_{pe} \approx 4.5 \times 10^{-2}$, in good agreement with the experiment. However, the code WAKE shows that the electron temperature does not affect so much the plasma frequency: Changing the temperature from 0 to 50 eV leads to a period shift of a few 10^{-3} , which is ten times less than the simple model. In addition, the fact that the shift disappears after a few periods indicates that it does not come from the electron temperature, and that the above simple model might overestimate the wave number k . The plasma period can also be modified when the electrons of the EPW reach relativistic velocities [17]. This shift has recently been observed by Modena *et al.* in SRLWF [18]. The increase of the electron mass induces a decrease of the frequency (negative shift). Our simulations show that the velocities of the electrons do not exceed $v/c \approx 0.1$ (at $n_e = 10^{16} \text{ cm}^{-3}$), which leads to a shift of only -0.25% . For multiple dimension oscillations, two other effects induce a frequency modification. When an electron has an elliptic motion, current loops and magnetic field are produced [19]. The magnetic field deflects the electron motion to third order in amplitude, which induces a decrease of the electron plasma frequency. In the case of nonlinear cylindrical electrostatic oscillations [13], the radial displacement of an electron away from the center of symmetry produces a charge density at the center which is greater than in planar geometry. This produces a stronger restoring electric field and leads to an increase (positive shift) of the electron plasma frequency [$\Delta\omega_p/\omega_{pe} \approx (\delta r/r_0)^2/12$, where δr is the electron displacement from its initial position r_0 , and $\delta r/r_0 \ll 1$]. The total frequency shift depends on the relative amplitudes of the thermal, the relativistic, the electrostatic, and the magnetic effects, or in other words, on the oscillation geometry and amplitude. In the context of the laser beat-wave accelerator, Bell and Gibbon [20]

have shown that these effects can have similar amplitudes and comparable spatial profiles. The code WAKE includes all these effects. Both measurements and simulations indicate that the electrostatic effect (frequency increase) is predominant in this experiment.

From the numerical fit presented in the previous paragraph, we have also deduced the damping rate γ . It is presented in Fig. 4 as a function of the background density n_e . The empty triangles are the results of the code WAKE. At high electron density ($>10^{17} \text{ cm}^{-3}$), the damping is very slow (tens of periods) and our measurements have not been made to sufficiently late times to give a precise measurement of γ . The solid line is a linear fit and shows that γ/ω_p decreases roughly like $1/n_e$. Several mechanisms can attenuate the oscillation. One of them is the fine scale mixing [13]: The frequency of the oscillations depends on their amplitudes (cf. Figs. 2 and 3). Electrons with different equilibrium radii have different frequencies. After some time, crossings of electrons can occur and induce a damping. With a maximum frequency shift of 5% at $n_e = 10^{16} \text{ cm}^{-3}$, electrons should appear with opposite phases after at least ten periods, which is five times longer than the observed damping. Another possible mechanism is the convection: The density perturbation propagates at the group velocity $v_g = \partial\omega/\partial k$, where $\omega^2 = \omega_{pe}^2 + 2k^2 v_{th}^2$. It reaches the edge of the focus after $T_C (= 2/\gamma) \approx \sigma/v_g$. Assuming $k \approx 2/\sigma$, the characteristic normalized attenuation rate should be $2\pi\gamma/\omega_{pe} \approx 24\pi(v_{th}^2/\sigma^2\omega_{pe}^2)$. It is linear with the electron density and equal to 0.6 for $n_e = 10^{16} \text{ cm}^{-3}$, $T_e = 50 \text{ eV}$, and σ , in good agreement with the experiment. However, this model is very crude, and simulations made in a preionized homogeneous plasma show a much slower attenuation (ten times slower at 10^{16} cm^{-3}), indicating that neither the convection nor the fine scale mixing can explain the observed damping. A good agreement is obtained only if we take into account the ionization of the gas. Two simulations made at $n_e = 10^{16} \text{ cm}^{-3}$ are presented in Fig. 5, one in a preformed homogeneous plasma

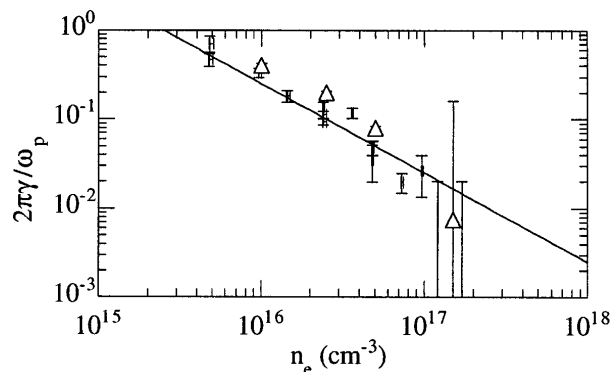


FIG. 4. Damping rate of the electron oscillation versus the electron density. The empty triangles are the results of the code WAKE. The solid line is a A/n_e fit.

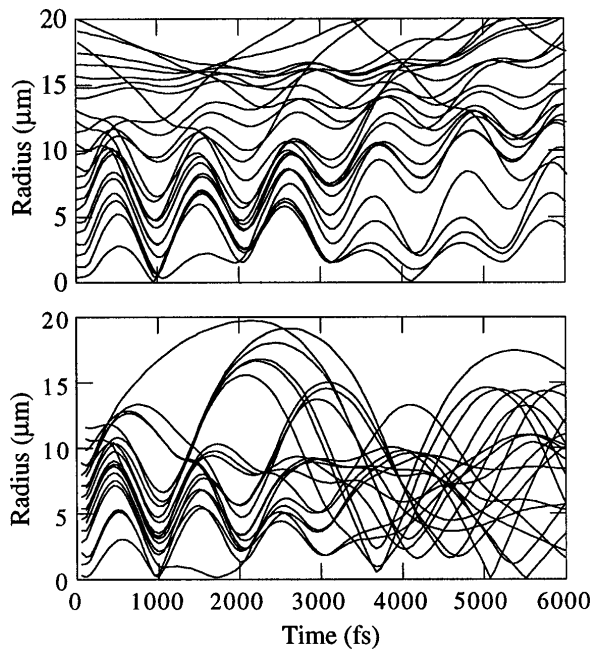


FIG. 5. Radial electron trajectories at the focal plane versus time obtained from the code WAKE. The top graph is in a homogeneous preformed plasma, while the bottom graph is in a plasma created by tunneling ionization of a helium gas.

(top graph), and the other in a tunneled-ionized helium gas (bottom graph). They show the electron radial trajectories at the laser focal plane. At time = 0, the electrons begin to feel the ponderomotive force of the pump laser pulse and move away from the focus. After the laser pulse, the electrons are pulsed back by the electrostatic field and oscillate at the plasma frequency. In the homogeneous plasma, this oscillation decreases quietly with time. In the case of a plasma created by tunneling ionization, two steep density gradients exist: at the $\text{He}^{2+}/\text{He}^+$ and the $\text{He}^+/\text{vacuum}$ interfaces. When it is pushed by the ponderomotive force of the laser pulse, an electron close to the $\text{He}^{2+}/\text{He}^+$ interface can explore the He^+ region or the vacuum. Thus it does not follow the collective motion of the EPW and can come back into the plasma after a few oscillations of the EPW. These electrons are not in phase with the EPW and destroy the oscillation. This damping mechanism is more important at low density because the electron excursion increases with $\delta n/n$ (cf. Fig. 2). Let us note that it is a little bit slower (two times at 10^{16} cm^{-3}) in a cold plasma but still remains important. A similar plasma edge effect has been observed in PIC simulations by Bonnaud *et al.* [21] in the case of an EPW excited in a planar geometry (longitudinal LWF) and in a cold plasma.

In conclusion, we have presented the first observation of the damping of an electron plasma oscillation excited by the laser wake-field process. The damping time (ex-

pressed in electron plasma periods) is linear with the electron density. It goes from two periods at $5 \times 10^{15} \text{ cm}^{-3}$ to tens of periods for densities above 10^{17} cm^{-3} . Our simulations suggest that the presence of a steep density gradient at the focus edge leads to the oscillation destruction. The frequency of the oscillations becomes larger than the linear electron plasma frequency for nonlinear EPW amplitudes. This constitutes the first observation of the frequency modification associated with nonlinear electrostatic oscillations excited in cylindrical geometry. Let us note that the plasma frequency increase and damping mechanisms we describe in this paper should not appear in the LWF accelerators, the electron oscillation of the EPW being longitudinal in that case.

It is a pleasure to acknowledge the help from G. Gillon and G. Rey for laser operation. This work has been supported by the Centre National de la Recherche Scientifique and by the EU Large Facility Program under Contract No. CHGE CT930021.

- [1] See, e.g., *Advanced Accelerator Concepts*, edited by P. Schoessow, AIP Conf. Proc. No. 335 (AIP, New York, 1995).
- [2] T. Tajima and J.M. Dawson, Phys. Rev. Lett. **43**, 267 (1979).
- [3] N.E. Andreev *et al.*, JETP Lett. **55**, 571 (1992); T.M. Antonsen, Jr. and P. Mora, Phys. Rev. Lett. **69**, 2204 (1992); P. Sprangle *et al.*, Phys. Rev. Lett. **69**, 2200 (1992).
- [4] Y. Kitagawa *et al.*, Phys. Rev. Lett. **68**, 48 (1992).
- [5] C.E. Clayton *et al.*, Phys. Rev. Lett. **70**, 37 (1993).
- [6] N.A. Ebrahim, J. Appl. Phys. **76**, 7645 (1994).
- [7] F. Amiranoff *et al.*, Phys. Rev. Lett. **74**, 5220 (1995).
- [8] K. Nakajima *et al.*, Phys. Rev. Lett. **74**, 4428 (1995).
- [9] A. Modena *et al.*, Nature (London) **377**, 606 (1995); C. Coverdale *et al.*, Phys. Rev. Lett. **74**, 4659 (1995).
- [10] E. Esarey and P. Sprangle, IEEE Trans. Plasma Sci. **24**, 252 (1996).
- [11] J.R. Marquès *et al.*, Phys. Rev. Lett. **76**, 3566 (1996).
- [12] C.W. Siders *et al.*, Phys. Rev. Lett. **76**, 3570 (1996).
- [13] J.M. Dawson, Phys. Rev. **113**, 383 (1959).
- [14] S. Augst *et al.*, Phys. Rev. Lett. **63**, 2112 (1989).
- [15] L.M. Gorbunov and V.I. Kirsanov, Sov. Phys. JETP **66**, 290 (1987).
- [16] P. Mora and T.M. Antonsen, Jr., Phys. Plasmas **4**, 217 (1997).
- [17] M.N. Rosenbluth and C.S. Liu, Phys. Rev. Lett. **29**, 701 (1972).
- [18] A. Modena *et al.*, IEEE Trans. Plasma Sci. **24**, 289 (1996).
- [19] L. Gorbunov, P. Mora, and T.M. Antonsen, Jr., Phys. Rev. Lett. **76**, 2495 (1996).
- [20] A.R. Bell and P. Gibbon, Plasma Phys. Controlled Fusion **30**, 1319 (1988).
- [21] G. Bonnaud *et al.*, Europhys. Lett. **26**, 91 (1994).